JOURNAL OF THERMOPHYSICS AND HEAT TRANSFER
Vol. 6, No. 3, July–Sept. 1992

Fixed Conductance Heat Pipe Performance with a Liquid Slug

R. P. Bobco* and B. L. Drolen†
Hughes Aircraft Company, Los Angeles, California 90009

Fixed conductance heat pipes (FCHPs) filled with working fluid at low or moderate temperatures develop a volume of excess liquid when operated at high temperatures. The excess liquid forms as either a puddle or a slug at the coldest end of the condenser and creates a temperature differential between the evaporator and the condensor end cap. Simple algebraic expressions are presented for predicting the thermal performance of an FCHP operating with a liquid slug formed by the combined influence of liquid density temperature dependence and meniscus depression. Both differential and two-node models are developed to account for condensation modeled either as a constant flux process or based on an isothermal vapor with a constant internal film coefficient. Numerical examples are included to illustrate the behavior of two axially grooved pipes operating over a range of heat loads with both real and ideal fluids. Prediction of evaporator temperature and liquid slug length is observed to have a weak dependence on the choice of model and mode of condensation and a strong dependence on real fluid effects.

Nomenclature

A_a = cross-sectional area within outside periphery, $A_w + A_v + A_c$
A_c = geometrical cross-sectional area of capillary structure (total groove area)
$\bar{A}_c$ = liquid-filled cross section of capillary structure (mean value based on meniscus depression)
A_v = geometrical vapor flow cross-sectional area (liquid slug cross section)
$\bar{A}_v$ = enlarged vapor flow cross-sectional area when meniscus depression occurs, $A_c + A_v = \bar{A}_c + \bar{A}_v$
A_w = conduction cross-sectional area of pipe wall
B_s = two-node model nondimensional fin parameter, $b_1^2(1 - \zeta_s)/2(1 - fK_v)$
b_1 = nondimensional fin parameter, $(h_0\ell/k_w)(S_0\ell/A_w)^{1/2}$
f = condensation flux parameter
G_s = nondimensional total liquid node conductance parameter
h_i = internal film coefficient
h_0 = external film coefficient or contact conductance
K^2 = nondimensional axial conductance ratio, k_wA_w/k_aA_a
K_v = nondimensional film coefficient, $h_iS_i/(h_iS_i + h_0S_0)$
k_a = "apparent" thermal conductivity of liquid-filled capillary structure
k_f = thermal conductivity of liquid
k_w = thermal conductivity of pipe wall
L = end-cap-to-end-cap length of heat pipe
ℓ = length of condenser section
ℓ_s = length of active condenser section (i.e., location of liquid slug interface)
m = mass of liquid charge in heat pipe
Q = heat load carried by vapor leaving evaporator section, W
q = condensation heat flux, W/m²
r, s = linearized liquid density temperature coefficients
S_i = liquid wetted perimeter of heat pipe interior
S_0 = external perimeter of heat pipe in contact with heat sink
$T(\zeta)$ = local temperature of heat pipe wall, Kelvin
T_0 = reference temperature at which liquid fills capillary passages with no liquid puddle or slug, Kelvin
T_v = vapor temperature, Kelvin
z = axial distance measured from transport section/condenser interface
α = ratio of condenser end-cap area to peripheral heat sink interface area, $A_a/S_0\ell$
α_v = ratio of liquid slug cross section to internal peripheral area of condenser section, $A_v/S_i\ell$
β_1^2 = generalized fin parameter for active condenser, $b_1^2/(1 - fK_v)$
β_2^2 = generalized fin parameter for liquid slug-filled condenser section, $b_1^2K^2$
ζ = nondimensional condenser location, z/ℓ
ζ_s = nondimensional length of active condenser, ℓ_s/ℓ
ρ = liquid density
τ = heat pipe forcing function, Kelvin
Φ = nondimensional slug interface conductance for two-node model
ϕ = liquid-to-wall axial conductance ratio in liquid slug zone, $k_f(A_v + A_c)/k_wA_w$

Introduction

THE fixed conductance heat pipe (FCHP) is a useful component in many spacecraft thermal control systems. In some applications, a FCHP is modeled as an isothermal element in a multinode simulation of a thermal control system; the uniform temperature of the FCHP is found to be proportional to the heat load applied at the evaporator and to depend on the heat sink temperature and conductance at the condenser. Such uniform temperature models are not appropriate in the presence of either evaporator "dryout" or excess liquid in the condenser. The present study examines a limiting case of the second condition, the influence of a liquid slug on the temperature distribution in an FCHP.

The phenomenon of excess liquid in an FCHP is described by Eninger and Edwards[1] and by Meyer et al.[2] Eninger and Edwards[1] present an analytical development, based on physical chemistry and hydrostatics, that shows how liquid slugs and liquid puddles form in a heat pipe operating in a gravity

Presented as Paper 90-1794 at the AIAA/ASME 5th Joint Thermophysics and Heat Transfer Conference, Seattle, WA, June 18–20, 1990; received July 25, 1990; revision received Oct. 1, 1991; accepted for publication Oct. 5, 1991.

*Retired. Fellow AIAA.
†Senior Staff Engineer, Space and Communications Group. Member AIAA.

field. The discussion is limited to meniscus shapes, and an application to priming arteries is discussed; no insights are provided on how slugs or puddles influence heat transfer characteristics or local temperatures in an FCHP. Meyer et al.[2] provide a qualitative description of slug and puddle formation in a zero-gravity environment and include temperature data from an FCHP experiment on an orbiting satellite. The authors identify temperature-dependent liquid density (liquid density varies inversely with temperature) and meniscus depression (i.e., the decrease in liquid area flow cross section in a capillary passage) as the primary causes of excess liquid; no analytical details are provided on the problem of performance prediction.

In most spacecraft applications, an FCHP must operate over a range of heat loads and heat sink temperatures. If the capillary passages are filled to capacity (without excess) at a high temperature, a liquid deficit may be observed when the pipe is operated at a low temperature; a liquid deficit contributes to evaporator dryout at low heat loads and/or low heat sink temperature operation. To preclude low temperature dryout, heat pipe manufacturers frequently fill pipes at temperatures several degrees below their minimum design temperature. At high-temperature operation, the combination of liquid density decrease and meniscus depression causes excess liquid to accumulate in the coldest region of the condenser, either as a puddle or as a slug. The excess liquid impedes heat transfer from the vapor core to the condenser wall and may lead to excessive evaporator temperatures or large axial temperature gradients near the condenser end cap or both.

The present study examines a simplified form of the problem of excess liquid in an FCHP. The analysis considers liquid slugs only, and their influence on FCHP axial temperatures. Liquid slugs seem to represent the stable configuration in a zero-gravity environment[2] and will exist in some terrestrial applications[1] as well. Both liquid density variation and meniscus depression are included in the mass balance, but the numerical results emphasize density variation. Meniscus depression is difficult to predict except in simple capillary structures (e.g., axial grooves).

The objective of this study is to develop a formulation for predicting the performance of an FCHP operating with a liquid slug in the cold end of the condensor. The formulation describes the conservation principles, boundary conditions, and numerous parameters required to make performance predictions for a fixed conductance heat pipe. The formulation requires a heat balance on the pipe walls and a mass balance on the liquid fill. Closed form temperature solutions are developed for both a differential model and a two-node model; for each model, condensation is assumed to occur at interior condenser surfaces, either with a constant flux or across a uniform film from an isothermal vapor. Evaporator wall temperature is taken as the dependent variable of primary interest, and the heat load leaving the evaporator is treated as the independent variable. The formulation for FCHP performance is similar to formulations for variable conductance heat pipes (VCHPs).[3,4] Numerical results for pipes of two different geometries illustrate the application of the four analytical formulations.

Analytical Models

The FCHP configuration examined here is shown in Fig. 1. The pipe has an end-to-end length L and a condenser section of length ℓ. The evaporator and condenser sections are separated by an adiabatic transport section (i.e., no heat loss from pipe exterior surface). The closed end of the condenser is assumed to be filled by a cylindrical slug of liquid of length $\ell - \ell_s$ and cross section A_v. Vapor crossing the evaporator/transport section interface is assumed to carry a heat load of Q watts; in the absence of losses in the transport section, condensation is assumed to be initiated in the condenser at $z = 0$. Condensation occurs at all interior surfaces

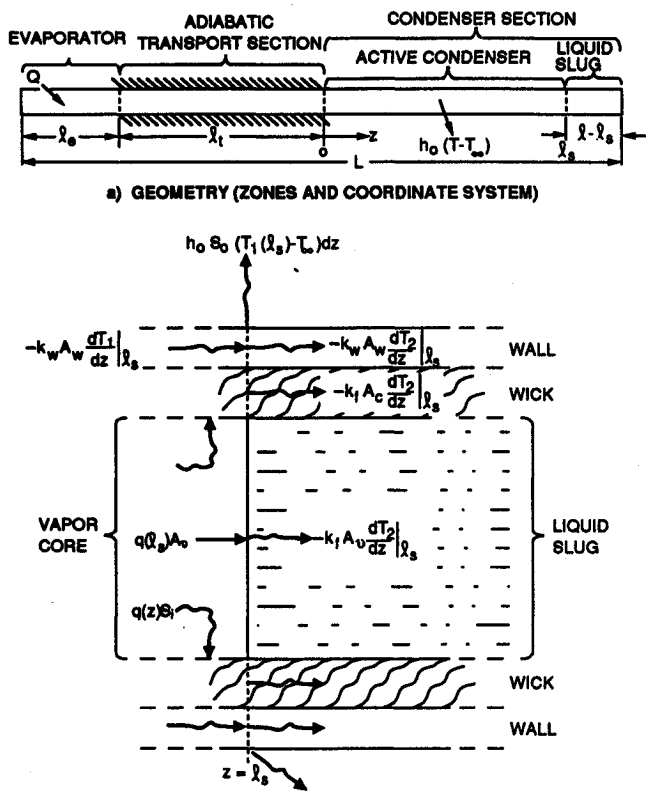

a) GEOMETRY (ZONES AND COORDINATE SYSTEM)

b) HEAT BALANCE COMPONENTS AT IDEALIZED LIQUID SLUG/VAPOR CORE INTERFACE, $z = \ell_s$

Fig. 1 Subject FCHP configuration.

of the condenser, including the capillary structure and condensed liquid surfaces. A heat balance on the vapor core may be expressed as

$$Q = S_i \int_0^{\ell_s} q(z)\, dz + q(\ell_s)A_v \tag{1}$$

where S_i is the interior wetted periphery and $q(z)$ is the local condensation heat flux; it is assumed that the condensation heat flux at the surface of the liquid slug is identical to the heat flux at the periphery adjacent to the slug. A more detailed description of condensation on the slug freesurface is not called for here because the assumption has little bearing on the key result; namely, evaporator temperature. The condensation heat flux is transported through the heat pipe wall and the liquid slug to a heat sink operating at a temperature T_∞.

The analysis of heat transport presented herein assumes that one-dimensional, steady heat transfer by conduction occurs in the pipe wall and the liquid slug; that the interior condensation process occurs either 1) with a uniform heat flux $q(z) = q$, or 2) with a uniform internal film coefficient from an isothermal vapor $q(z) = h_i(T_v - T(z))$; that the heat sink temperature and the external film coefficient h_0 are uniform over the length of the condenser and the exterior end cap area A_e; that the thermal conductivities of the wall and condensed liquid k_w and k_f, respectively, are constant at all axial locations; that axial conduction in the capillary passages is negligible in the active condenser section $(k_wA_w) >> (k_f\bar{A}_c)$, $0 < z \leq \ell_s$; that there is no noncondensable gas in the internal pipe volume; that the liquid charge in the pipe completely fills the capillary volume with no excess liquid at a reference temperature T_0, (i.e., $m = \rho[T_0]A_cL$); that axial conduction is negligible in the adiabatic transport section, $dT/dz = 0$, $z \leq 0$; that the influence of a meniscus can be neglected at the liquid slug surface; and that the liquid is at the same temperature as the adjacent pipe wall, both in the capillary struc-

ture and the liquid slug. Additional assumptions are identified in the course of the analytical development.

Four different analytical models are examined within the framework of the preceding assumptions 1) a constant flux differential model (in which condensation flux is assumed uniform at all interior condenser surfaces); 2) an isothermal vapor differential model (in which vapor temperature and internal film coefficient are assumed uniform in the active condenser); 3) a two-node constant flux model; and 4) a two-node isothermal vapor model. These models are used to find the evaporator wall temperature as a function of heat load when account is taken of the liquid slug at the closed end of the condenser. The analysis starts by considering the differential formulation:

Field Equation $0 < z \leq \ell$

$$0 < z \leq \ell_s, \quad k_w A_w \frac{d^2T_1}{dz^2} - h_0 S_0 (T_1 - T_\infty) = -S_i q(z) \tag{2a}$$

$$\ell_s < z \leq \ell, \quad k_a A_a \frac{d^2T_2}{dz^2} - h_0 S_0 (T_2 - T_\infty) = 0 \tag{2b}$$

where

$$k_a A_a = k_w A_w + k_f (A_v + A_c) \tag{2c}$$

Boundary Conditions $z = 0, \ell$

$$z = 0, \quad dT_1/dz = 0 \tag{3a}$$

$$z = \ell, \quad -k_a A_a \frac{dT_2}{dz} = h_0 A_a [T_2(\ell) - T_\infty] \tag{3b}$$

Matching Conditions $z = \ell_s$

$$T_1(\ell_s) = T_2(\ell_s) \tag{4a}$$

$$-k_w A_w \left.\frac{dT_1}{dz}\right|_{\ell_s} + q(\ell_s) A_v = -k_a A_a \left.\frac{dT_2}{dz}\right|_{\ell_s} \tag{4b}$$

Heat Balance on Vapor Mass

Constant Flux

$$Q = q(S_i \ell_s + A_v) \tag{5a}$$

Isothermal Vapor

$$Q = h_i S_i \int_0^{\ell_s} [T_v - T_1(z)]\, dz + h_i A_v [T_v - T_i(\ell_s)]$$

$$= h_i S_i \ell_s (T_v - \bar{T}_1) + h_i A_v [T_v - T_1(\ell_s)] \tag{5b}$$

The location of the interface between the active condenser and the liquid slug ℓ_s is unknown in the preceding equations. An independent equation in ℓ_s can be obtained by considering the distribution of liquid and vapor in the heat pipe:

$$\rho_v(T_0) A_v L + \rho(T_0) A_c L = \bar{A}_c \left[\rho(T_e)(L - \ell) + \int_0^{\ell_s} \rho(T)\, dz\right] + (A_c + A_v) \int_{\ell_s}^{\ell} \rho(T)\, dz + \bar{A}_v (L - \ell + \ell_s) \rho_v(T_v) \tag{6}$$

The integrals on the right side of Eq. (6) cannot be integrated in closed form in the general case because liquid density is nonlinear in temperature and temperature is transcendental in z. The mean value theorem can be invoked to integrate Eq. (6) in principle

$$\rho_v(T_0) A_v L + \rho(T_0) A_c L = \bar{A}_c [\rho(T_e)(L - \ell) + \bar{\rho}_1 \ell_s] + (A_c + A_v) \bar{\rho}_2 (\ell - \ell_s) + \bar{A}_v (L - \ell + \ell_s) \rho_v(T_v) \tag{7}$$

where $\bar{\rho}_1$ and $\bar{\rho}_2$ are mean liquid densities in the active condenser and the slug, respectively. Fortuitously, for many heat pipe fluids, including anhydrous ammonia NH_3, liquid density decreases as a nearlinear function of temperature over a useful temperature range:

$$\rho(T) = r - sT, \quad T_0 < T \leq T_{\max} \tag{8}$$

For this special case, mean liquid density is a simple function of mean temperature:

$$\bar{\rho}_i = \frac{1}{z_{i+1} - z_i} \int_{z_i}^{z_{i+1}} (r - sT)\, dz = r - s\bar{T}_i \tag{9}$$

Using Eq. (9) in Eq. (7) and rearranging terms leads to a simple algebraic expression for ℓ_s

$$\zeta_s = \frac{\ell_s}{\ell} = \frac{\left[\frac{A_v}{A_c} - \left(\frac{L}{\ell} - 1\right)\left(1 - \frac{\bar{A}_c}{A_c}\right)\right] + \left(\frac{s}{r}\right)\left[T_0\left(\frac{L}{\ell}\right) - T_e\left(\frac{L}{\ell} - 1\right)\left(\frac{\bar{A}_c}{A_c}\right) - \bar{T}_2\left(1 + \frac{A_v}{A_c}\right)\right] + X}{\left[\frac{A_v}{A_c} + \left(1 - \frac{\bar{A}_c}{A_c}\right)\right] + \left(\frac{s}{r}\right)\left[\bar{T}_1\left(\frac{\bar{A}_c}{A_c}\right) - \bar{T}_2\left(1 + \frac{A_v}{A_c}\right)\right] - Y}$$

where

$$X = \left(\frac{L}{\ell} - 1\right)\left(\frac{\bar{A}_v}{A_c}\right)\frac{\rho_v(T_v)}{r} - \left(\frac{L}{\ell}\right)\frac{A_v}{A_c}\frac{\rho_v(T_0)}{r}$$

$$Y = \left(\frac{\bar{A}_v}{A_c}\right)\frac{\rho_v(T_v)}{r} \tag{10}$$

The meniscus depression ratio $\bar{A}_c/A_c$ appears as a parameter in Eq. (10). In the absence of a meniscus $\bar{A}_c/A_c = 1$ while for typical capillary structures operating under a heat load $\bar{A}_c/A_c < 1$. The case $\bar{A}_c/A_c > 1$ has been shown by Meyer et al.[2] not to be a stable case in zero gravity; that is the excess liquid forms a slug, not a film. This case is possible in 1 g reflux operation, the flooding limit, but the current model is not valid for reflux mode. The present formulation treats $\bar{A}_c/A_c$ as a known parameter; a more rigorous treatment would cast the meniscus depression as another dependent variable requiring a parallel solution for fluid flow and, thus, pressure drop, yielding pressure difference between vapor and liquid as a function of axial position. This would certainly not allow for a simple closed-form solution, such as that given here. Eq. (10) is used in the remaining analysis to illustrate analytical procedures and trends. To simplify the following analysis, vapor mass in the heat pipe core is assumed to be negligible. In this case, $X = Y = 0$ in Eq. (10). This is a reasonable assumption at low-to-moderate operating temperatures and is conservative at high operating temperatures.

The two-node formulation postulates that the heat pipe envelope is isothermal everywhere between the evaporator end-cap and the active condenser/slug interface $z = \ell_s$. The temperature of the liquid slug is assumed to decrease linearly between the condenser/slug interface and the condenser end-

cap. The following heat balance equations must be solved to obtain the two nodal temperatures:

Active Condenser $0 < z \leq \ell_s$

$$q_l S_i \ell_s = h_0 S_0 \ell_s (T_1 - T_\infty) + \frac{2k_w A_w}{(\ell - \ell_s)} (T_1 - T_2) \quad (11a)$$

Liquid Slug $\ell_s < z \leq \ell$

$$\frac{2k_w A_w}{(\ell - \ell_s)} (T_1 - T_2) + q_s A_v = h_0 S_0 (\ell - \ell_s)(T_2 - T_\infty) + U_2 A_a (T_2 - T_\infty) \quad (11b)$$

where

$$1/U_2 A_a = (\ell - \ell_s)/2k_a A_a + 1/h_0 A_a \quad (11c)$$

The condensation fluxes q and q_s are equal for the constant flux model; the isothermal vapor model requires

$$q_1 = h_i (T_v - T_i) \quad (12a)$$

$$q_s = U_s (T_v - T_2) \quad (12b)$$

$$1/U_s = A_v [(\ell - \ell_s)/2k_f (A_v + A_c) + 1/h_i A_v] \quad (12c)$$

The liquid mass balance given by Eq. (7) or Eq. (10) applies to the two-node model by virtue of the fact that $T_1 = T_e = \bar{T}_1$ and $T_2 = \bar{T}_2$. The following analyses lead to general temperature solutions for the differential and two-node models that apply for both the constant flux and isothermal vapor condensation cases.

Analysis

For the purpose of algebraic convenience, a number of parameters appearing in Eqs. (1–12) are combined in nondimensional groups. At the same time, the field equations, heat balance equations, forcing functions, and so forth are reduced to have dimensions of absolute temperature. A condensation parameter f is introduced to make the solutions applicable both for the constant flux and isothermal vapor cases:

$$f = \begin{cases} 0, & \text{constant flux} \\ 1, & \text{isothermal vapor} \end{cases} \quad (13a)$$

The forcing functions for the two condensation cases are

$$\tau = \begin{cases} (qS_i/h_0 S_0), & \text{constant flux} \\ K_v (T_v - T_\infty), & \text{isothermal vapor} \end{cases}$$

or

$$\tau = (1 - f)(qS_i/h_0 S_0) + fK_v (T_v - T_\infty) \quad (13b)$$

where

$$K_v = h_i S_i / (h_0 S_0 + h_i S_i) \quad (14a)$$

The remaining parameters common to both the differential and two-node models are

$$\begin{aligned} \zeta &= z/\ell, \quad \zeta_s = \ell_s/\ell, \quad b_1^2 = (h_0 \ell / k_w)(S_0 \ell / A_w) \\ \phi &= k_f (A_v + A_c)/k_w A_w \\ K^2 &= k_w A_w / k_a A_a = 1/(1 + \phi) \\ \alpha &= A_a / S_0 \ell, \quad \alpha_v = A_v / S_i \ell \end{aligned} \quad (14b)$$

$$\begin{aligned} \tau_s &= K_v [T_1(\zeta_s) - T_\infty] \\ \beta_1^2 &= b_1^2/(1 - fK_v) \\ \beta_2^2 &= b_1^2 K^2 = \beta_1^2 K^2 (1 - fK_v) \end{aligned}$$

The differential formulation takes the following form:

Field Equation $0 < \zeta \leq 1$

$$0 < \zeta \leq \zeta_s, \quad \frac{d^2 T_1}{d\zeta^2} - \beta_1^2 (T_1 - T_\infty) = -\beta_1^2 \tau \quad (15a)$$

$$\zeta_s < \zeta \leq 1, \quad \frac{d^2 T_2}{d\zeta^2} - \beta_2^2 (T_2 - T_\infty) = 0 \quad (15b)$$

Boundary Conditions $\zeta = 0, 1$

$$dT_1/d\zeta|_0 = 0 \quad (16a)$$

$$-dT_2/d\zeta|_1 = \alpha \beta_2^2 [T_2(1) - T_\infty] \quad (16b)$$

Matching Conditions $\zeta = \zeta_s$

$$T_1(\zeta_s) = T_2(\zeta_s) \quad (17a)$$

$$-dT_1/d\zeta|_{\zeta_s} + \beta_1^2 \alpha_v \tau = -\frac{1}{K^2} (dT_2/d\zeta)_{\zeta_s} + f\beta_1^2 \alpha_v \tau_s \quad (17b)$$

Integrating Eqs. (15a) and (15b) and using the boundary conditions defined in Eq. (16), find

$$T_1(\zeta) - T_\infty = \tau (1 + A_1 \cosh \beta_1 \zeta) \quad (18a)$$

$$T_2(\zeta) - T_\infty = \tau A_2 [\cosh \beta_2 (1 - \zeta) + \alpha \beta_2 \sinh \beta_2 (1 - \zeta)] \quad (18b)$$

The constants of integration A_1 and A_2 must be evaluated from the matching conditions Eq. (17). In condensed notation A_1 and A_2 can be found from the matrix equation

$$\begin{vmatrix} \cosh \beta_1 \zeta_s & -U_2 \\ W_1 & (\beta_2 V_2 / \beta_1 K^2) \end{vmatrix} \cdot \begin{vmatrix} A_1 \\ A_2 \end{vmatrix} = \begin{vmatrix} -1 \\ \beta_1 A_v (1 - fK_v) \end{vmatrix} \quad (19)$$

Table 1 Hypothetical heat pipe dimensions and properties

Parameter	FCHP P1	FCHP P2
Geometry		
Outer diameter (d_0), cm	NA	0.9800
Vapor core diameter (d_v), cm	1.3465	0.6450
Total pipe length (L), m	0.7808	1.00
Condenser length (ℓ), cm	22.86	8.00
Internal wetted periphery (S_i), cm	4.2301	2.026
External periphery (S_0), cm	7.62	3.078
Pipe wall cross section (A_w), cm^2	1.3432	0.3226
Vapor core cross section (A_v), cm^2	1.4264	0.3265
Capillary flow cross section (A_c), cm^2	0.4548	0.1052
Total pipe cross section (A_a), cm^2	3.2245	0.7542
Internal condenser area ($S_i \ell$), cm^2	96.768	16.210
External condenser area ($S_0 \ell$), cm^2	174.19	24.632
Properties		
Pipe wall thermal conductivity (k_w), W/m-°C	192.1	
Liquid ammonia thermal conductivity (k_f), W/m-°C	0.4309	
Liquid ammonia density modulus (s/r), K^{-1}	1.414×10^{-3}	
Condenser/sink conductance (h_0), W/m^2-°C	2389	
Internal condensation coefficient (h_i), W/m^2-°C	5679	

$$\left.\begin{aligned} U_2 &= \cosh \beta_2(1-\zeta_s) + \alpha\beta_2 \sinh \beta_2(1-\zeta_s) \\ V_2 &= \sinh \beta_2(1-\zeta_s) + \alpha\beta_2 \cosh \beta_2(1-\zeta_s) \\ W_1 &= \sinh \beta_1\zeta_s + f\beta_1 K_v\alpha_v \cosh \beta_1\zeta_s \end{aligned}\right\} \quad (20)$$

A_1 and A_2 follow as

$$\left.\begin{aligned} A_1 &= \beta_2(\alpha_v\beta_2 U_2 - V_2)/D \\ A_2 &= \beta_1 K^2(\sinh \beta_1\zeta_s + \beta_1\alpha_v \cosh \beta_1\zeta_s)/D \\ D &= \beta_1 K^2 U_2 W_1 + \beta_2 V_2 \cosh \beta_1\zeta_s \end{aligned}\right\} \quad (21)$$

Equations (18) and (21) represent the temperature distribution in an FCHP when the internal condensation forcing function is specified by Eqs. (13a) and (13b). The mean temperatures follow as

$$\bar{T}_i = \int_{\zeta'}^{\zeta''} T_i(\zeta)\, d\zeta/(\zeta'' - \zeta')$$

$$= T_\infty + \tau(1 + (A_1/\beta_1\zeta_s)\sinh \beta_1\zeta_s) \quad (22a)$$

$$\bar{T}_2 = T_\infty + \tau[A_2/\beta_2(1-\zeta_s)](\sinh \beta_2(1-\zeta_s)$$

$$+ \alpha\beta_2[\cosh \beta_2(1-\zeta_s) - 1]) \quad (22b)$$

The differential formulation is completed by evaluating the forcing function components from Eq. (5)

$$(qS_i/h_0S_0) = Q/h_0S_0\ell(\zeta_s + \alpha_v) \quad (23a)$$

$$K_v(T_v - T_\infty) = Q/h_0S_0\ell\hat{D} \quad (23b)$$

$$\hat{D} = (\zeta_s + \alpha_v) - [A_1K_v/\beta_1(1-K_v)]$$

$$\cdot (\sinh \beta_1\zeta_s + \beta_1\alpha_v \cosh \beta_1\zeta_s) \quad (23c)$$

The performance of an FCHP operating with a liquid slug adjacent to the condenser end-cap can be established by a simultaneous solution for Eq. (18a) for evaporator temperature $T_e = T_1(0)$; Eq. (22a) for active condenser mean temperature $\bar{T}_1$; Eq. (22b) for liquid slug mean temperature $\bar{T}_2$; and Eq. (10) for the liquid slug interface location ζ_s.

For purposes of comparison it is useful to examine the performance of an FCHP whose capillary passages are filled, exactly, with an ideal fluid. An ideal fluid, as defined here, has a liquid density that is independent of temperature and is not susceptible to meniscus depression ($\bar{A}_c/A_c = 1$). The temperature distribution in such an FCHP can be found from Eq. (18a) by setting $\zeta_s = 1$ and $K = 1$ to evaluate the constant of integration A_1. The forcing function τ for an ideal fluid requires setting $\zeta_s = 1$ in Eqs. (23a), (23b), and (23c), as well. Finally, it is of interest to observe a limiting case for an ideal fluid that arises for the condition of an adiabatic condenser end-cap. In this instance, the boundary condition defined by Eq. (16b) reduces to $(dT/d\zeta)_{\zeta=1} = 0$ and leads to the result $A_1 = 0$, $T(\zeta) =$ constant in $0 < \zeta \leq 1$. The ideal fluid with adiabatic end-cap leads to the intuitive result $T_1(\zeta) - T_\infty = \tau$, from Eq. (15a).

The two-node formulation yields a solution for T_1 and T_2 after rearrangement of Eqs. (12a) and (12b) and introduction

Table 2 Nondimensional parameters for liquid slug analysis

Parameter	Symbol	FCHP P1	FCHP P2
Normalized pipe length	(L/ℓ)	3.4156	12.5
Vapor core-to-capillary ratio	(A_v/A_c)	3.1362	3.1157
Vapor core-to-interior condenser ratio	α_v	0.01475	0.02015
Total cross section-to-external condenser ratio	α	0.07404	0.03062
Fluid-to-wall conductance ratio	ϕ	0.003142	0.002999
Wall-to-total conductance ratio	K	0.9984	0.9985
Internal film coefficient fraction	K_v	0.81621	0.56826
Active condenser fin parameter			
Constant flux ($f = 0$)	β_1	10.4656	0.4989
Isothermal vapor ($f = 1$)	β_1	24.412	14.4564

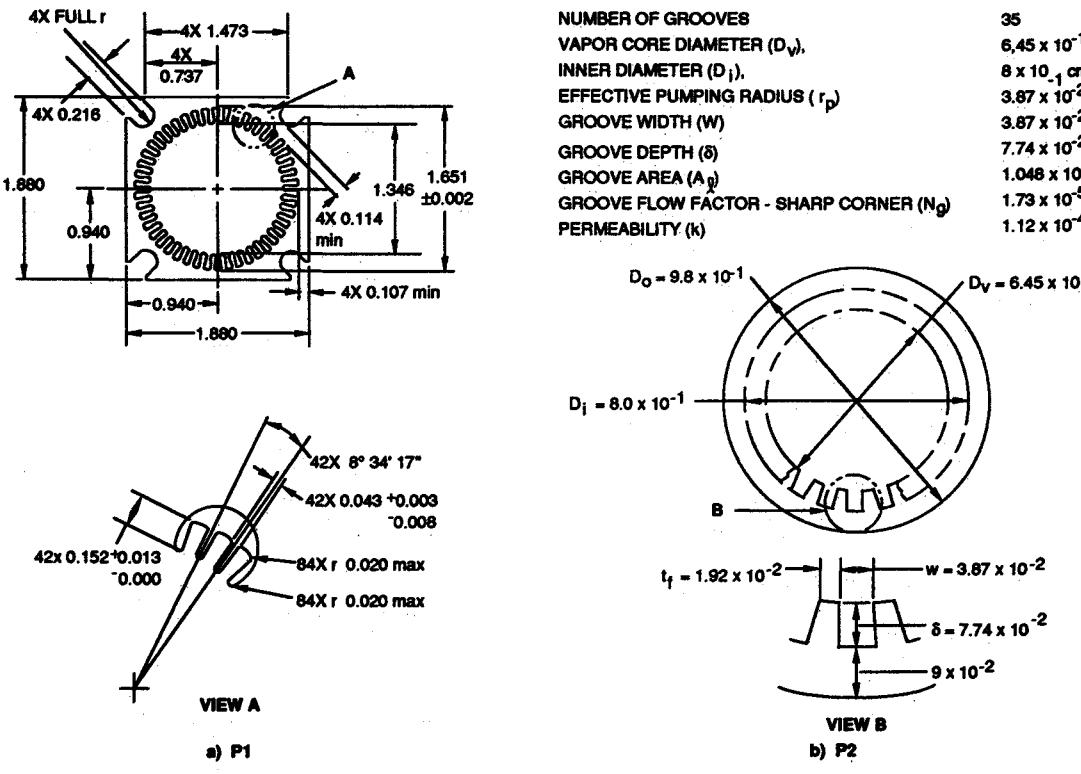

Fig. 2 Hypothetical heat pipe cross sections.

Table 3 Constants of integration and vapor temperature: differential formulations ($\bar{A}_c/A_c = 1$)

Q, W	Isothermal vapor ζ_s	Isothermal vapor $\frac{A_1}{\cosh \beta_1 \zeta_s}$	Isothermal vapor A_2/β_2	$(T_v - T_\infty)$ °C	Constant flux ζ_s	Constant flux $\frac{A_1}{\cosh \beta_1 \zeta_s}$	Constant flux A_2/β_2
			P1				
0	0.9267	−0.2001	0.03907	0	0.9267	−0.4073	0.02895
50	0.9156	−0.2023	0.03488	5.06	0.9152	−0.4108	0.02566
100	0.9042	−0.2041	0.03103	10.23	0.9034	−0.4135	0.02268
150	0.8925	−0.2055	0.02752	15.52	0.8913	−0.4157	0.01998
200	0.8806	−0.2067	0.02433	20.95	0.8789	−0.4174	0.01755
250	0.8683	−0.2076	0.02143	26.53	0.8661	−0.4188	0.01537
300	0.8558	−0.2083	0.01882	32.26	0.8531	−0.4199	0.01340
350	0.8230	−0.2089	0.01647	38.16	0.8396	−0.4207	0.01165
400	0.8298	−0.2093	0.01435	44.24	0.8258	−0.4213	0.01008
			P2				
0	0.7301	−0.2902	0.00894	0	0.7301	−0.4028	0.00752
10	0.7124	−0.2907	0.00756	3.28	0.7111	−0.4034	0.00629
20	0.6940	−0.2910	0.00635	6.73	0.6913	−0.4038	0.00521
30	0.6747	−0.2913	0.00529	10.36	0.6703	−0.4041	0.00426
40	0.6542	−0.2915	0.00436	14.21	0.6478	−0.4043	0.00344

Table 4 Predicted evaporator temperatures for real and ideal fluids (differential models, no meniscus depression [$\bar{A}_c/A_c = 1$])

Q, W	Real fluid: Isothermal vapor ζ_s	Real fluid: Isothermal vapor $(T_e - T_\infty)$, °C	Real fluid: Constant flux ζ_s	Real fluid: Constant flux $(T_e - T_\infty)$, °C	Ideal fluid: Isothermal vapor ζ_s	Ideal fluid: Isothermal vapor $(T_e - T_\infty)$, °C	Ideal fluid: Constant flux ζ_s	Ideal fluid: Constant flux $(T_e - T_\infty)$, °C	Ideal fluid: Insulated end cap ζ_s	Ideal fluid: Insulated end cap $(T_e - T_\infty)$, °C
					P1					
0	0.9267	0	0.9267	0	1.0	0	1.0	0	1.0	0
50	0.9156	4.13	0.9152	4.35	1.0	3.83	1.0	3.98	1.0	4.04
100	0.9042	8.35	0.9034	8.81	1.0	7.67	1.0	7.97	1.0	8.08
150	0.8925	12.67	0.8913	13.39	1.0	11.51	1.0	11.96	1.0	12.14
200	0.8806	17.10	0.8789	18.10	1.0	15.34	1.0	15.94	1.0	16.18
250	0.8683	21.65	0.8661	22.95	1.0	19.17	1.0	19.92	1.0	20.23
300	0.8558	26.33	0.8531	27.96	1.0	23.01	1.0	23.91	1.0	24.28
350	0.8230	31.14	0.8396	33.13	1.0	26.28	1.0	27.89	1.0	28.32
400	0.8298	36.12	0.8258	38.48	1.0	30.68	1.0	31.88	1.0	32.37
					P2					
0	0.7301	0	0.7301	0	1.0	0	1.0	0	1.0	0
10	0.7124	1.87	0.7111	1.96	1.0	1.39	1.0	1.40	1.0	1.43
20	0.6940	3.82	0.6913	4.02	1.0	2.79	1.0	2.81	1.0	2.86
30	0.6747	5.89	0.6703	6.22	1.0	4.18	1.0	4.21	1.0	4.29
40	0.6542	8.08	0.6478	8.57	1.0	5.58	1.0	5.61	1.0	5.72

of three additional nondimensional parameters:

$$B_s = \tfrac{1}{2}b_1^2(1 - \zeta_s)/(1 - fK_v) = \tfrac{1}{2}\beta_1^2(1 - \zeta_s) \quad (24a)$$

$$G_s = (1 - \zeta_s)(1 - fK_v) + \frac{\alpha(1 - fK_v)}{1 + B_sK^2\alpha(1 - fK_v)} + fK_v \quad (24b)$$

$$\Phi = \frac{\phi\alpha_v}{\phi + fK_v\alpha_vB_s} \quad (24c)$$

Using Eq. (24) in Eq. (11), the nodal heat balance equations can be cast in matrix form:

$$\begin{vmatrix} (1 + B_s\zeta_s) & -1 \\ -1 & (1 + B_sG_s) \end{vmatrix} \cdot \begin{vmatrix} (T_1 - T_\infty) \\ (T_2 - T_\infty) \end{vmatrix} = B_s\tau \begin{vmatrix} \zeta_s \\ \Phi \end{vmatrix} \quad (25)$$

The solution for T_1 and T_2 yields

$$(T_1 - T_\infty) = \tau[1 + (\Phi - G_s)/D_2] \quad (26a)$$

$$(T_2 - T_\infty) = (\tau/D_2)[\zeta_s + (1 + B_s\zeta_s)] \quad (26b)$$

$$D_2 = \zeta_s + B_s\zeta_sG_s + G_s \quad (26c)$$

The set the yields a simultaneous solution for FCHP performance consists of Eq. (26a) for evaporator temperature $T_e = T_1$; Eq. (26a) for active condenser mean temperature $\bar{T}_1 = T_1$; Eq. (26b) for liquid slug mean temperature $\bar{T}_2 = T_2$; and Eq. (10) for liquid slug interface location ζ_s. The application of the differential and two-node formulations is illustrated below, where the performance of ammonia/aluminum FCHPs of two different configurations is examined.

Numerical Examples

The formulations developed above are applied here to the prediction of the performance of two aluminum FCHPs assumed to be operating over a range of heat loads and in environments that cause a liquid slug to form. Both pipes use NH_3 as the working fluid and have axially grooved capillary passages. The hypothetical heat load ranges are not necessarily attainable; that is, the pumping capacity of each capillary structure may be limited to heat loads that are lower than some of those examined here. Axially grooved wick structures are assumed because the liquid passage cross section A_c is geometrically well defined. While wall wicks of screen or metal felt are not excluded from the present formulations, some degree of empiricism and/or subjectivity is required to estimate A_c, $\bar{A}_c$, and the axial thermal conductivity

of such wicks. The present formulations must be modified before they can be applied to FCHPs with helical grooves, a monogroove, or slab wicks.

For convenience, the FCHPs examined here are designated P1 and P2. P1 is a pipe being developed by the Hughes Electron Dynamics Division for a spacecraft application; P2 is a hypothetical pipe described by Brennan and Kroliczek.[5] The dimensions and assumed thermal properties of each pipe are summarized in Table 1. A cross-sectional view of each is shown in Fig. 2. P1 has a conventional internal circular cross section with axial grooves and a square external cross section. In operation, only one face of the external periphery is coupled to a heat sink; the three remaining faces are assumed to be adiabatic. The geometrical periphery of P1 is 7.62 cm, but the "thermal periphery," $S_0 = 1.905$ cm must be used in the performance equations. Coupling to the heat sink is assumed to occur across a thin epoxy bond with a conductance $h_0 = 2839$ W/m²-°C. P2 has an outer diameter $d_0 = 0.98$ cm and is assumed to be thermally coupled to a heat sink over its full periphery $S_0 = 3.078$ cm with a conductance, $h_0 = 2839$ W/m²-°C. The condenser end cap of each pipe is assumed to be coupled to the heat sink over an area proportional to the peripheral contact. The pipes are assumed to have the following features in common: an internal film coefficient $h_i = 5679$ W/m²-°C;[5] a heat sink temperature $T_\infty = 21°C = 294$ K; a reference temperature for liquid mass $T_0 = -6.7°C = 266.3$ K; and NH_3 density modulus $(s/r) = 1.414 \times 10^{-3}$ K ($200 \text{ K} < T \leq 350$ K, based on $\rho[T]$ tabulations).[5] Several nondimensional parameters are tabulated in Table 2 for use in Eqs. (14b) and (24). Meniscus depression was neglected ($\bar{A}_c/A_c = 1$) to establish baseline results for comparing analytical models. Subsequently, limited calculations were made for P1 using $\bar{A}_c/A_c = 0.90$.

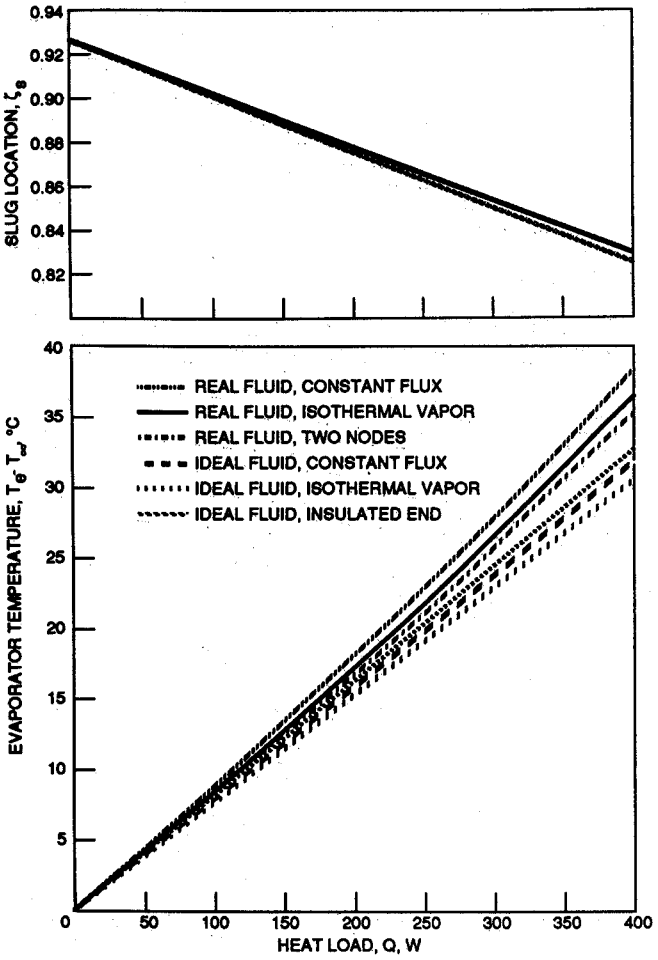

Fig. 3 Slug interface locations and evaporator temperatures for P1 with real and ideal fluids (differential and nodal models, no meniscus depression ($\bar{A}_c/A_c = 1$)).

The differential formulation (Eqs. (18a), (23a), (23b), (10), etc.) requires an iterative procedure for solution because the temperatures are transcendental in ζ_s. The equations were coded for a programmable hand calculator, and performance characteristics were found for each FCHP. Input data consisted of the following: (A_v/A_c), (s/r), (L/ℓ), α_v, α, K, K_v, T_0, T_∞, b_1, f, $(h_0 S_0 \ell)$, and Q. A trial value of ζ_s(in) was used to calculate temperatures which, in turn, were used to calculate ζ_s(out). If ζ_s(out) $\neq \zeta_s$(in), ζ_s(out) was used as a second trial value, and the calculations were repeated. In general, input/output parity in ζ_s was obtained in fewer than 10 iterations. Output data of interest for a specified Q included ζ_s, T_e, $\bar{T}_1$, $\bar{T}_2$, A_1, A_2, and T_v ($f = 1$, only).

The two-node formulation also was coded for an iterative solution using a programmable hand calculator. In principle, the two-node formulation can be arranged to obtain a quadratic equation in ζ_s, but this possibility was not exploited in the present study. Inputs for the nodal formulation were comparable to those for the differential model; the only outputs of interest were ζ_s, T_1, T_2, and T_v($f = 1$, only).

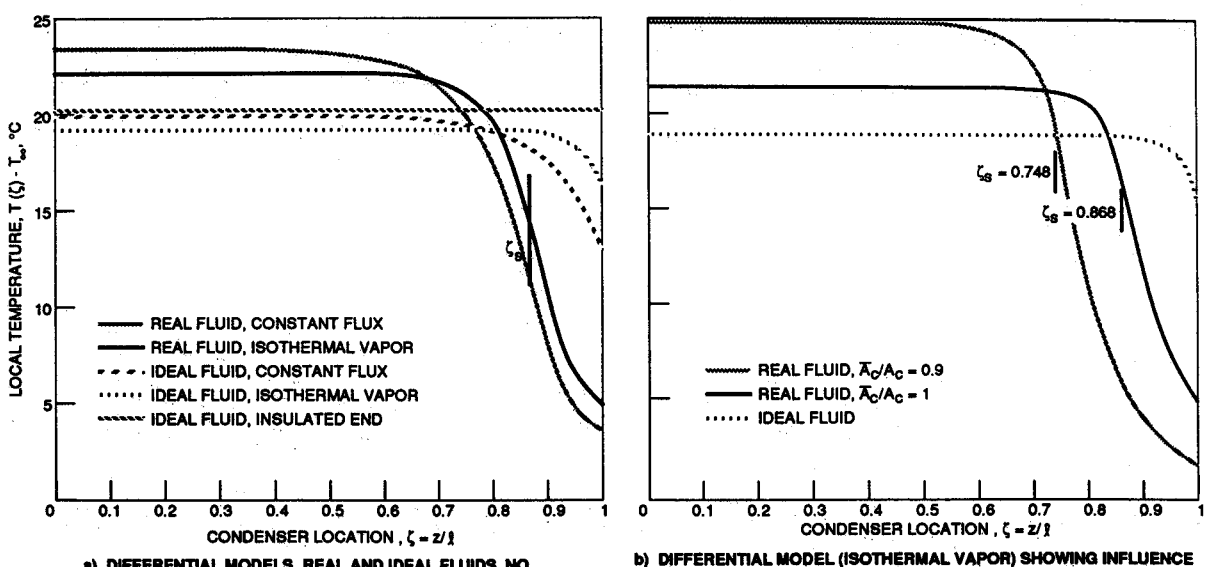

Fig. 4 P1 Axial temperature distribution $Q = 250$ W.

Calculations for P1 were made over the range $0 \leq Q \leq 400$ W. For P2, calculations were made for the range $0 \leq Q \leq 40$ W. Constants of integration for the differential formulation are shown in Table 3. Temperatures for four different analytical models of the same FCHPs are shown in Fig. 3 (P1 only). The differential formulation was used to calculate evaporator temperatures using an ideal fluid; that is, a working fluid whose density is independent of temperature. These results are presented in Fig. 3 and Table 4. The final column of Table 4 contains results for the condition of an insulated end-cap; this condition leads to an isothermal heat pipe surface that is independent of the condensation assumption.

Fig. 4a shows axial temperature profiles for P1 operating with a heat load $Q = 250$ W. Temperature profiles are shown for both types of condensation (i.e., constant flux and isothermal vapor) and for real and ideal fluids. The liquid slug occurs at $\zeta_s \approx 0.869$ for a real fluid (NH_3); there is no slug for an ideal fluid. The influence of meniscus depression is illustrated in Fig. 4b, where axial temperature profiles are shown for $Q = 250$ W based on the differential model with isothermal vapor. Temperature profiles are shown for 1) an ideal fluid; 2) a real fluid with liquid density dependence only ($\bar{A}_c/A_c = 1$); and 3) a real fluid with both density dependence and meniscus depression ($\bar{A}_c/A_c = 0.90$). The constants of integration for the last case are $A_1 = -0.21051$, $A_2 = 0.00611$, and $(T_v - T_\infty) = 30.43$°C.

Discussion

The results obtained by applying the mathematical models described here illustrate the influence of a liquid slug on the performance of a fixed conductance heat pipe. Comparison of real and ideal fluid effects (see Table 4) shows that a liquid slug in the condenser will increase the evaporator temperature above the value predicted for an ideal fluid. The temperature increment due to a liquid slug is roughly proportional to the evaporator heat load; at low heat loads, the influence of a liquid slug is almost negligible, but at high heat loads a liquid slug may raise the evaporator temperature above an acceptable level. The evaporator temperature rises above an ideal value because the slug decreases the length of the condenser section available for heat transfer to a heat sink.

Comparison of two modes of condensation (see Tables 3 and 4) shows that the constant flux model predicts evaporator temperatures only slightly higher than those predicted by the isothermal vapor model. This small difference between the results for the two models is significant, because no results exist to indicate which model is more realistic. In general, the influence of real fluid liquid density is greater than the influence of condensation mode on predicted evaporator temperature. The agreement between the differential models and two-node models is very good (see Fig. 3). The two-node models predict mean temperatures in the active condenser that are assumed to be the same as evaporator temperatures. The assumption seems to be reasonable for the two FCHPs examined here. Additionally, it may be observed that the two-node models seem to be less sensitive to condensation mode than the differential models. Comparison of the evaporator temperatures predicted by the three ideal fluid models (see Table 4) discloses relatively minor differences. The simplest ideal fluid model (insulated end-cap) is more conservative than the differential models and seems to be adequate for purposes of preliminary design. Once more, it is important to note that ideal fluid models underestimate evaporator temperatures. Ideal fluid calculations should not be used when they predict evaporator temperatures that approach the upper temperature limit for any application.

The axial temperature profiles (see Fig. 4a) for the real fluid models show that a liquid slug in an FCHP creates a temperature distribution similar to that expected in a VCHP. Perfunctory examination of test data from an FCHP with a liquid slug could lead to the conclusion that gas generation had occurred in the pipe. Careful testing at elevated and reduced temperatures will differentiate between liquid and gas blockage due to the incompressibility of the liquid. A model consolidating the effects of both liquid and gas would be a desirable extension of the present work. It would, however, be subject to the unknown gas quantity in an FCHP, because the gas exists due to corrosion over heat pipe life. Examination of Fig. 4a also shows that the isothermal vapor model leads to prediction of a pipe wall temperature distribution in the active condenser that is more nearly isothermal than that predicted by the constant flux model. This condition occurs because the condensation flux increases along the length of the active condenser section $q(z) = h_i(T_v - T_i(z))$. It is reasonable to expect that in some capillary structures, the internal film coefficient will also increase with condensor location $h_i(z)$, making the pipe wall even more isothermal.

The influence of meniscus depression on axial temperature (see Fig. 4b) is quite strong. The assumption $\bar{A}_c/A_c = 0.9$ represents a near-maximum meniscus depression for the groove dimensions shown in Fig. 2 for P1. The results shown in Fig. 4b are intended to illustrate a trend rather than to provide an all-inclusive evaluation of meniscus depression. These exploratory results suggest that meniscus depression should not be neglected in predicting FCHP performance. The assumption of negligible vapor mass in the heat pipe core yields a conservatively large liquid slug size. This produces some exaggeration of the heat pipe temperature profile and a slight overprediction of evaporator temperatures. As a specific example, in the case of P1 with a 250 W heat load, the mass distribution in the heat pipe is roughly 78.5% in the capillaries, 14.5% in the liquid slug, and 7% in the vapor core.

The final observation on the comparisons reported here deals with the temperature of the liquid in the capillary passages of the evaporator, transport section, and active condenser. The formulation developed here postulates that liquid temperature is equal to wall temperature. This assumption seems to be reasonable for predicting FCHP performance in thermal control systems, but greater accuracy may be required when analyzing FCHP test data. Intuitively, the liquid condensed in axial grooves is at a temperature between the wall temperature and the vapor temperature; as an improved estimate the average may be useful. The result of weighting the liquid temperature to include both vapor and wall temperatures is to increase the volume occupied by liquid. That is, the length of a liquid slug observed in a tested FCHP will be slightly greater than that predicted by the present model.

Summary and Conclusions

Expressions have been derived to predict the performance of an FCHP operating with a liquid slug at the coldest end of the condenser section. They can be used to examine real or ideal working fluids, internal condensation based on an isothermal vapor or constant flux, and either a differential model or a two-node model of an FCHP. Two hypothetical heat pipes were analyzed to obtain insight into the influence of a liquid slug on FCHP performance and to compare the several models. A number of observations were made based on this analysis: that a liquid slug causes an increase in evaporator temperature above the value predicted without a liquid slug; that the axial temperature distribution in an FCHP condenser operating with a liquid slug is similar to the distribution caused by a noncondensable gas; that the isothermal vapor differential model predicts a slightly lower evaporator temperature than the constant flux differential model; that agreement between the evaporator temperatures and liquid slug lengths predicted by the differential and two-node models is good; that a simple FCHP model based on an ideal fluid and adiabatic end-cap can be used for preliminary design estimates, but that this model underestimates evaporator temperature and should not be used for high heat load performance predictions; and finally, that both liquid density de-

pendence on temperature and meniscus depression influence the length of a liquid slug and heat pipe performance.

Several recommendations can be made on the basis of the results reported here. Heat pipe design and fabrication information obtained by thermal analysts from the manufacturer should include mass of liquid fill; vapor flow cross section A_v; capillary cross-section A_c; and total length (or volume) of capillary passages. Finally, the work reported here indicates that additional experimental studies of FCHP performance with excess liquid are needed.

Acknowledgment

The authors gratefully acknowledge the assistance of George L. Fleischman of Hughes Electron Dynamics Division, who provided useful insights into the behavior of fixed conductance heat pipes operating with excess liquid.

References

[1]Eninger, J. W., and Edwards, D. K., "Excess Liquid in Heat Pipe Vapor Spaces," *Heat Transfer and Thermal Control Systems,* edited by L. S. Fletcher, Vol. 60, Progress in Astronautics and Aeronautics, AIAA, New York, 1978, pp. 80–95.

[2]Meyer, R., Laux, U., and Schlitt, R., "Excess Liquid Formation in Orbit Test Results of Axially Grooved Heat Pipes," *Journal of Spacecraft and Rockets,* Vol. 23, No. 5, Sept.–Oct. 1986, pp. 482–486.

[3]Bobco, R. P., "Variable Conductance Heat Pipe Performance Analysis: Zero-to-Full Load," *Journal of Thermophysics and Heat Transfer,* Vol. 3, No. 1, Jan. 1989, pp. 33–41.

[4]Bobco, R. P., "VCHP Performance Prediction—A Comparison of First Order and Flat Front Models," *Journal of Thermophysics and Heat Transfer,* Vol. 3, No. 4, Oct. 1989, pp. 401–405.

[5]Brennan, P. J., and Kroliczek, E. J., *Heat Pipe Design Handbook,* NASA NAS 5-23405, June 1979.